Thermal behavior of Pd@SiO 2 nanostructures in various gas environments: a combined 3D and in situ TEM approach

Walid Baaziz, Mounib Bahri, Anne Sophie Gay, Alexandra Chaumonnot, Denis Uzio, Sébastien Valette, Charles Hirlimann, Ovidiu Ersen

Thermal behavior of $Pd@SiO_2$ nanostructures in various gas environments: a combined 3D and in-situ TEM approach

Walid Baaziz,[1]* Mounib Bahri,[1] Anne Sophie Gay,[2] Alexandra Chaumonnot,[2] Denis Uzio,[2] Sébastien Valette,[3] Charles Hirlimann[1] and Ovidiu Ersen[1,4,5,]*

[1] Institut de Physique et Chimie des Matériaux de Strasbourg (IPCMS), UMR 7504, CNRS - Université de Strasbourg, 23 rue du Lœss BP 43, 67034 Strasbourg cedex 2, France

[2] IFP Énergies Nouvelles (IFPEN) Lyon, Rond-point de l'échangeur de Solaize, BP 3, 69360 Solaize, France

[3] Centre de Recherche en Acquisition et Traitement de l'Image pour la Santé (CREATIS), UMR 5220 – INSERM U1206, Université Lyon 1 – INSA Lyon - Université Jean Monnet Saint-Etienne, 7 Avenue Jean Capelle O, 69100 Villeurbanne, France

[4] University of Strasbourg Institute for Advanced Studies (USIAS), Strasbourg, France

[5] Institut Universitaire de France (IUF), Paris, France

* corresponding authors

Abstract

The thermal stability of core-shell $Pd@SiO_2$ nanostructures was for the first time monitored by using *in-situ* Environmental Transmission Electron Microscopy (E-TEM) at atmospheric pressure coupled with Electron Tomography (ET) on the same particles. The core Pd particles, with octahedral or icosahedral original shapes were followed during a thermal heating under gas at atmospheric pressure. In a first step, their morphology/faceting evolution was investigated under reductive H_2 environment up to 400°C by electron tomography performed on the same particles before and after the *in situ* treatment. As a result, we observed the formation of small Pd particles inside the silica shell due to the thermally activated diffusion from the core particle. A strong dependence of the shape and faceting transformations on the initial structure of the particles was evidenced. The octahedral monocrystalline NPs were found to be less stable than the icosahedral ones, in the first case the Pd diffusion from the core towards the silica external surface lead to a progressive decrease of the particles size. The icosahedral polycrystalline NPs do not exhibit morphology/faceting change, as in this case the atom diffusion within the particle is favored against diffusion towards the silica shell, due to a high amount of crystallographic defects in the particles.

In the second part, the $Pd@SiO_2$ NPs behavior at high temperatures (up to 1000 °C) was investigated under reductive or oxidative conditions; it was found to be strongly related to the thermal evolution of the silica shell: (1) under H_2, the silica is densified and losses its porous structure leading to a final state with Pd core NPs encapsulated in the shell; (2) under air, the silica porosity is maintained and the increase of the temperature leads to an enhancement of the diffusion mechanism from the core towards the external surface of the silica; as a result, at 850 °C all the Pd atoms are expulsed outside the silica shell.

Introduction

In the general context of the heterogeneous catalysis process, one of the most important classes of catalysts, from both a fundamental and an industrial point of view, is based on palladium-supported nanoparticles. They are generally used for catalysing various chemical processes such as CO oxidation,[1,2,3] NO_x reduction,[4,5] hydrogenation,[6,7,8] and dehydrogenation.[9] However, such catalysts are generally unstable at high reaction temperatures and their activity rapidly decays.[10,11] Indeed, to increase the catalytic activity, the palladium nanoparticles (NPs) as any metal, should display a size of a few nanometers (usually less than 10 nm) in order to enhance the number of surface active sites.[12,13,14,15,16] Sintering and/or agglomeration are among the most important deactivation causes of nanoparticle catalysts due to an irreversible increase of the particle size resulting from a localized heating and a high thermal energy.[17]

To address these problems, considerable effort was devoted to developing new generations of palladium based-catalysts with original "sintering-resistant" properties such as core@shell structures consisting of a metallic palladium core encapsulated in a porous oxide shell.[18,19,20,21,22,23] It was recently shown that silica as a shell can stabilize metal particles and improve the thermal stability of catalysts against sintering.[22,24,25,26,27,28,29] Park et al. reported that Pd@SiO_2 remains stable up to 700 °C and yields a better catalytic activity than classical Pd/SiO_2 catalysts for CO oxidation.[22] J. Martins et al. used successfully Pd@SiO_2 as a catalyst for the CO_2 hydrogenation reaction and showed that the encapsulation of Pd with a silica shell has a beneficial impact on the stability of the NPs against sintering.[30] A. Forman showed that compared to traditional Pd/SiO_2, the core-shell Pd@SiO_2 displays a significantly higher activity and longer on-stream lifetime for the C_2H_2 hydrogenation. However, Pd@SiO_2 as a "new catalyst" was usually studied in terms of catalytic performances: only seldom papers presented advanced characterization of these nanostructures in order to understand their thermal stability, selectivity dependence from the shape/faceting and the mechanisms/phenomena leading to deactivation.

In the characterization framework of heterogeneous catalysis, the evolution of the catalyst microstructure and/or morphology and size is usually studied by Transmission Electron Microscopy (TEM) via observations made on several parts of the sample before and after the catalytic reaction. A few years ago, new generations of Environmental-TEM (E-TEM) cells were developed that allow the *in situ* study of the dynamical behavior of nanomaterials at high temperature and pressure up to the atmospheric pressure.[31] In comparison with the conventional dedicated E-TEM usually operating in vacuum (up to 30 mbar) the E-TEM cells offer the opportunity to work at atmospheric pressure (~1 bar), which dramatically influences the kinetics of the studied reactions. Otherwise, catalysts investigations usually need data such as dispersion of the active phase on the support, pores distribution, accessibility and the 3D morphology that cannot be acquired through 2D images; the most suited technique to access to this kind of information is Electron Tomography (ET). Therefore, combining E-TEM with ET appears as a promising very powerful tool allowing a complete and reliable insight of the catalyst evolution under realistic conditions. In the literature, such E-TEM-ET coupling was performed only by a few groups in dedicated microscopes for investigating the dynamical behaviour of nanomaterials such as the oxidation effect on bimetallic alloys at high temperature with tomographic series acquired before and after the in-situ experiment,[32] or for following *in situ* and in three dimension (3D) the calcination of silver nanoparticles supported on silica zeolites using a more complex approach based on rapid tomography acquisitions during the in-situ experiment.[33]

This work is at the interface between the development of new characterization tools and the understanding of material properties. We report on an original study that illustrates for the first time the experimental combination between E-TEM and ET techniques on the same objects and leads to results uncovering the thermal evolution of $Pd@SiO_2$ catalysts. Their behaviour is monitored as a function of their structure and type of gas environment under realistic conditions of pressure (1 atmosphere) for various catalytic reactions. In a first step, the thermal stability is investigated during a typical reduction treatment under H_2 at atmospheric pressure up to 400 °C. Such E-TEM-ET "unique object approach" allowed us to acquire 3D data related to the evolution of the morphology and faceting of the palladium particles during the reduction treatment. To obtain complementary information on their evolution at higher temperature, these nanostructures were also studied in a second step under H_2 and air environments, providing thus a complete insight on the atom diffusion mechanisms in such encapsulated 3D architectures.

Results and discussion

1. General characteristics of the $Pd@SiO_2$ nanostructures

The TEM images (Figure 1A and Figure 1SI) of the as synthesized $Pd@SiO_2$ particles show a relatively narrow size distribution of Pd NPs with a size of 17.2 ± 3.8 nm and the presence of generally one Pd particle and, in some rare cases, 2 or 3 particles, inside mesoporous silica shells that are 60-70 nm thick. Figure 1B presents a STEM-ADF (Scanning TEM, Annular Dark Field) image of typical $Pd@SiO_2$ particles evidencing the mesoporous texture of the silica shell made out of radial channels, but also the presence of some dispersed atomic Pd clusters (≤ 0.5 nm in size) probably originating from the residual K_2PdCl_4 used at the time of the synthesis process. The distribution of the palladium and silicon elements within the nanostructures was investigated using energy-dispersive X-ray spectroscopy (EDX) in STEM for mapping the Pd, Si and O elements (Figure 1C). The Pd and Si maps are consistent with the expected core-shell structures. The EDX map of palladium does not detect the presence of some possible clusters, due to their very small size which gives a poor signal to noise ratio in the chemical maps.

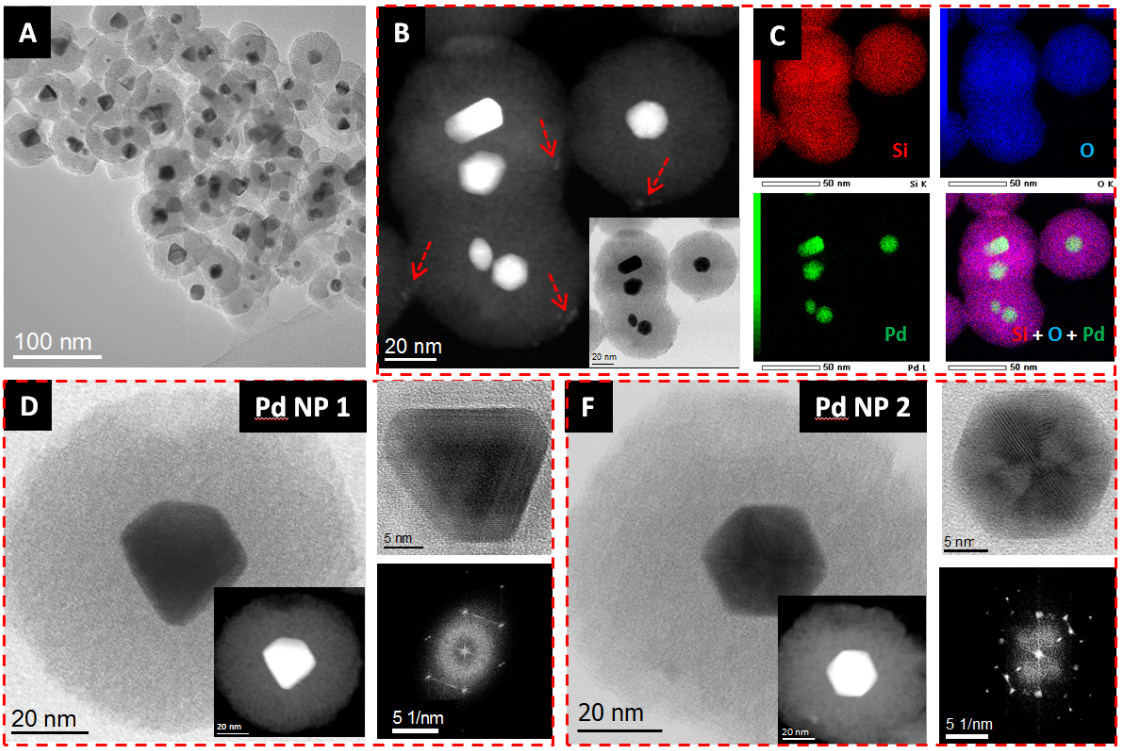

Figure 1. A) Typical TEM image of the Pd@SiO_2 catalyst, B) STEM ADF image (inset, STEM BF) of some representative Pd@SiO_2 particles, C) STEM EDX mapping of Si, O, Pd of the particles in B, D) and F) STEM BF and ADF, HR-TEM (inset, FFT) images of the two types of Pd@SiO_2 particles presents in the sample.

The TEM images do also reveal the presence of two types of core Pd particles: (1) monocrystalline particles with an octahedral shape (Figure 1D) with spots easily indexed to the reflections of the fcc lattice of Pd metal i.e 2.2 Å, 1.9 Å and 1.2 Å corresponding to the (111), (100) and (220) plans, respectively (JCPDS Card No. 05-0681), (2) icosahedral multiply twinned particles (MTPs) (Figure 1F), the twinned atomic plans and the FFT micrograph do confirm that these particles are polycrystalline with a major (111) external facet as reported in the literature.[34] The FFT present additional spots with a d_{hkl} distance of 3.4 Å, which could be the result of a moiré pattern. The presence of such two types of Pd particles can be explained by different growth kinetics due to the use of the CTAB as a capping agent.[35] Xiong Y. et al reported that MTPs Pd particles could be obtained following a blocking of the oxidative etching during the growth step.[34]

2. Thermal stability of Pd@SiO_2 during a reduction treatment (under H_2 up to 400 °C)

Before the *in situ* treatment under H_2, several zones with different magnifications were quickly visualized under argon at 200 °C in order to limit the contamination in STEM. Then, the cell was degassed and a H_2 flux was introduced at atmospheric pressure (760 torr); the temperature was subsequently increased to 400 °C with a heating rate of 5 °C.min^{-1} and kept for 30 min. Note that such experimental conditions are similar to that used to reduce catalysts in catalytic reactors.[30]

Figure 2 presents two areas characterized by ET before and after the *in situ* treatment under H_2. The areas were chosen to be representative of the sample with typical structures of the Pd@SiO_2 particles and one or two particles inside the silica shell, in order to be able to study the individual and the "more collective" thermal behaviour of the Pd particles, respectively.

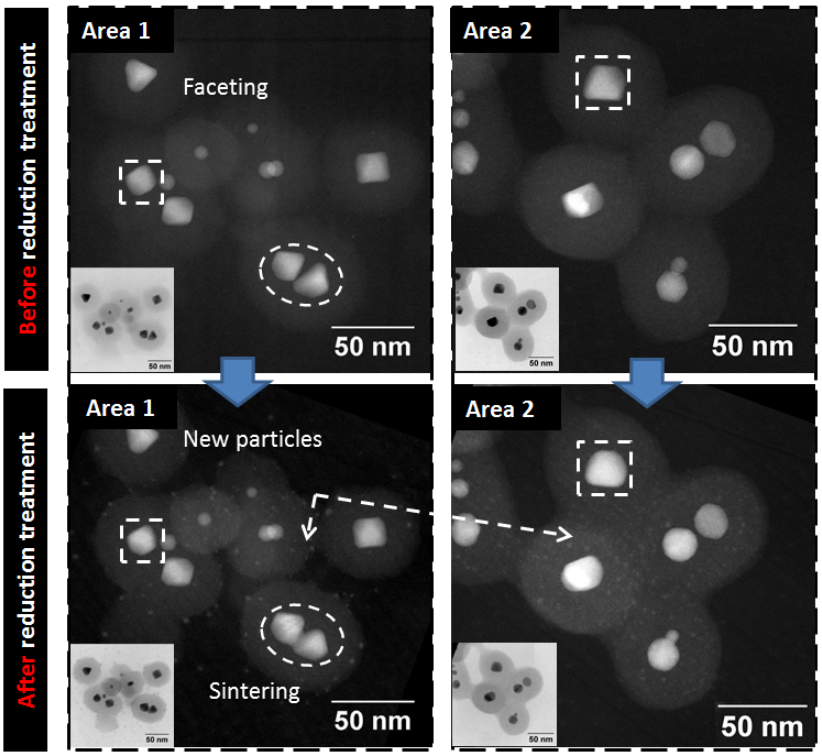

Figure 2. STEM-ADF (inset STEM-BF) images of two areas with Pd@SiO_2 particles (chosen for ET experiments) before and after the *in situ* reduction treatment. The images after reduction do reveal the presence of new small particles, the rough Pd NPs faceting evolution (squares) and the sintering trend of close octahedral NPs (circles).

The direct comparison of STEM images of the two areas before and after thermal treatment shows that the general appearance of the Pd@SiO_2 particles is preserved, nevertheless three major observations were highlighted: (1) the appearance of new small Pd particles in the silica shell (arrows), (2) a sintering-like and/or coalescence mechanism of some NPs when more than one Pd particle are present as cores inside the same silica shell (circles) and (3) a faceting evolution mainly in the case of monocrystalline NPs (squares). Alternately, it is known that the TEM electron beam may induce a local heating of the irradiated regions especially under gas (due to the gas ionisation effect) and could accelerate the evolution kinetics. In order to estimate the electron beam effect, only the area 2 was imaged during the *in situ* thermal treatment (the area 1 was not exposed to the electron beam during the thermal reductive treatment). There is only one noticeable difference between the continuously being irradiated area 2 and the protected area 1: the beam irradiation prevents the formation of large cluster on the surface of the particles.

2.1 Growth of new Pd particles within the silica shell

Electron tomography data including 3D volume, two typical (xy) slices and the 3D model obtained by segmenting the volume of the area 1 of Figure 2 after thermal treatment are shown on Figure 3 (two animations of the 3D models before and after the thermal treatment can be found in movie SI-1 and SI-2). Such data, especially the extracted slices, clearly show the presence of new small Pd particles with a size of 1±0.5 nm localized within the porous silica (xy slice 1) and some larger ones of about 3±0.5 nm on the external surface (xy slice 2). In the literature, only few groups reported such a mechanism for Pd@SiO_2 due to the fact that such particles are usually characterized by classical TEM in which the

contrast and the signal to noise ratio of small particles are not sufficient for them to be observed. Mc Farland et al. reported the presence of such "wall particles" (of 1.7 nm before and 3 nm after catalytic reaction) in Pd@SiO_2 catalyst for C_2H_2 hydrogenation but without explanation on their formation mechanism.[36] Similarly, "redispersion" of palladium was also reported by C. Y. Seo et al. in Pd@SiO_2 used as catalyst for CO oxidation at high temperature and was explained by a diffusion of Pd atoms followed by condensation upon cooling.[37]

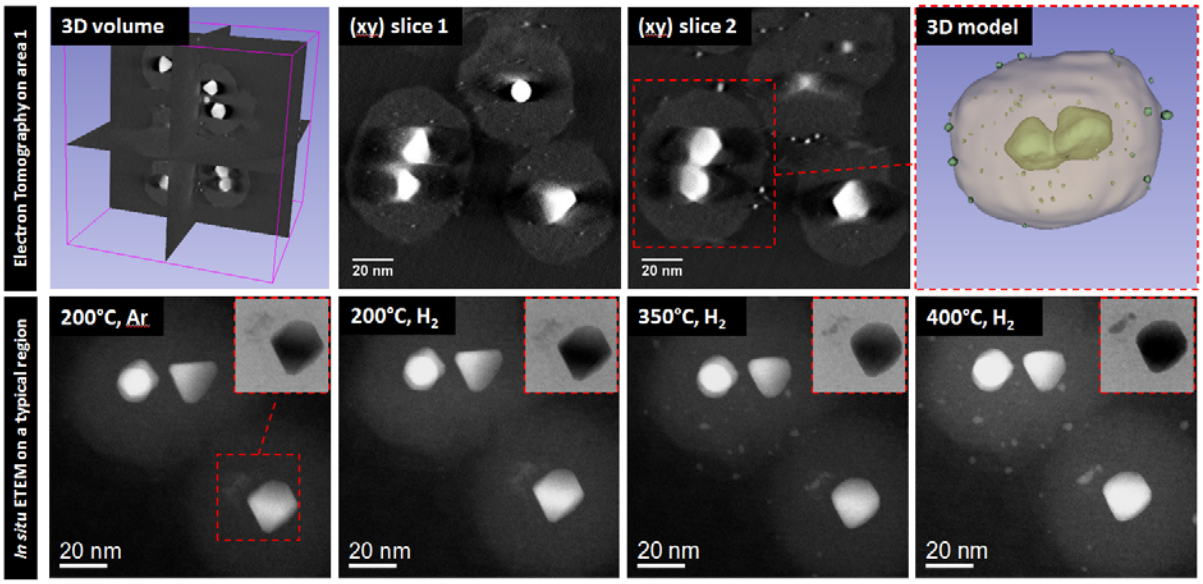

Figure 3. *Top*: 3D volume, two typical (xy) slices and 3D model (of the particles inside the red square) obtained by electron tomography carried out on particles from the area 1 in Figure 2. *Bottom*: STEM-ADF images of typical Pd@SiO_2 particles evolution during the *in situ* thermal treatment from 200 °C to 400 °C under H_2 gas at 760 torr, inset STEM-BF images of the highlighted region in red square.

The thermal evolution of Pd@SiO_2 particles in a typical region observed *in situ* is schematized on Figure 3 (*bottom*), more particles are shown in Figure 2SI. Above 300 °C, the TEM images show the formation of a large number of small Pd NPs in the inner part and on the external surface of the silica shells. The zone highlighted (in insets) illustrates the formation mechanism of such NPs between 200 °C and 400 °C, which appears as a dynamic coalescence/ripening resulting from the migration of Pd clusters initially present in the mesoporous silica. In addition, the formation of a large number of new Pd particles compared to the few clusters initially observed in the silica shell suggests the presence of an additional source of palladium. In such Pd@SiO_2 structures, two possible reservoirs could ensure such intake of palladium at high temperatures: (1) the presence of an important amount of residual palladium precursor in the silica shell and/or (2) the palladium core. To check the possible presence of K_2PdCl_4 inside the shell, several EDX spectra were recorded on large parts of silica that did reveal the presence of only Si and O peaks, no Pd, Cl, or K peaks were observed (Figure 3SI). As a result, we can presume that the new small particles can be formed first from the coalescence of the few clusters initially present in the silica shells but also, additionally, through a diffusion mechanism of palladium atoms from the core which aggregate on the Pd small particles already nucleated in the silica shell. In addition, the presence of new Pd NPs smaller than 2 nm inside the silica and bigger ones at the outer surface can be due to the fact that the ripening/growth process of new Pd NPs formed inside the silica is limited by the pores size (about 2.2 nm as reported in the ref **30**). Such observations suggest that, as a function of temperature, the first new NPs of palladium (of 1±0.5 nm) are formed inside the silica shell (at about 300 °C) via the coalescence of the clusters/diffusion from the

core and diffuse through the pores until the surface and then sintered to form the larger particles at the external surface (of 3±0.5 nm). Similar results were reported by De Jong et al. in the case of nickel precursors during calcination in SBA15 support. [38]

The mechanism of palladium diffusion from the core through silica was reported as a result of inter-diffusion and the formation of metal silicide via oxygen vacancies at the interfacial region between Pd and Si.[37,39] It is also known that palladium can react with hydrogen to form instable palladium hydride phase leading to increase the particles volume due to the incorporation of H2 into the palladium structure.[40,41] In our case, we suggest that the formation of such palladium hydride species occurred principally on the areas of palladium NPs surface in contact with the opened pores of silica shell, which can enhance the diffusion kinetic of palladium. We therefore expect the hydruration of the particles to only play a very marginal role in their morphology evolution. The diffusion orientation of the atoms from the core to the outside part of the silica shell can be explained also by a partial shrinkage of the silica shell, which leads to an additional stress on the Pd core. In a similar case, Forman et al. reported after catalytic tests an important agglomeration of silica shell leading to an increase of the size of the Pd particles formed within the silica from 1.7 nm to 3 nm.[36] In our case, using the ET results we can evidence that the larger 3 nm particles (in our case) are localized on the external surface of the silica shell. To investigate the shrinkage of the silica shells at 400 °C, we followed their sizes in the areas 1 and 2 (Figure 2) before and after the thermal treatment (see Figure 4SI), and we could evidence a slight size decrease of about 3-5 nm.

2.2 Thermal dependence of the shape/faceting of Pd particles during the reduction treatment

Most of the studies performed on Pd@SiO_2 reported a better resistance against sintering when the metal particles are encapsulated, regardless of the intrinsic microstructural properties of different Pd particles i.e size, morphology and faceting. In this work, further investigations were carried out using the "unique object approach" in order to discriminate the thermal evolution behaviour of the octahedral and icosahedral Pd particles observed in our case. Indeed, the morphological changes of the Pd@SiO_2 deduced from *in situ* E-TEM observations under H_2 at 400 °C reveals, qualitatively, the presence of more new Pd NPs on the external surface of silica shells containing octahedral Pd cores (area 1, Figure 2), while the particles with icosahedral Pd cores show almost only new small particles within the silica pores (area 2, Figure 2).

Figure 4 shows the thermal evolution of typical octahedral particles during the reduction treatment. The impact of the thermal treatment on the octahedral particles was studied by considering two particles inside the same silica shell from the area 1 and one particle from the area 2 (particles in red squares). The 3D models obtained through ET before and after the reduction treatment confirms the octahedral shape of the particles having 7-8 facets (see the 3D models, inset). After the thermal treatment, we observe that the global morphology is maintained, but a considerable downsizing was observed for the studied particles (as example, the particle in Figure 4 lost about 3 nm in size).

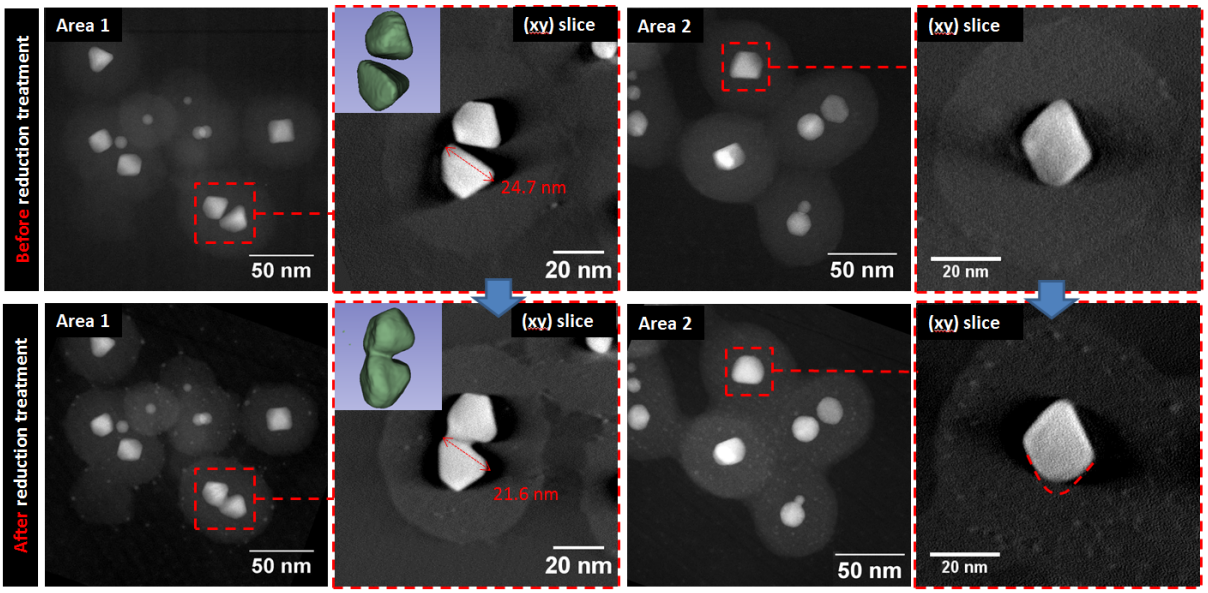

Figure 4. Octahedral Pd particles before (*top*) and after (*bottom*) the thermal treatment: *From Left to right:* (1) STEM-ADF images of the area 1, (2) a typical slice through the reconstruction of the two particles highlighted by red square in (1), in insets the 3D models, (3) STEM-ADF images of the area 2, (4) a typical slice through the reconstruction of the particle highlighted by red square in (3).

To better analyze the faceting, the external surface of the particles was separated in its corresponding facets, before and after the reduction treatment, using a geometrical approach based on the relative orientations of the normal axes between neighbouring surface voxels (for much details, see Experimental Part). The areas of well-identified facets of the two particles of area 1 were calculated and are presented in the Table 1SI (3D models are shown in movie SI-3 and movie SI-4). It is obvious that a direct comparison of the values obtained for the particles before and after the thermal treatment allows obtaining information on the evolution of the faceting in a more reliable way as compared to a basic visualization. In addition, from the segmented 3D reconstruction we could calculate a representative volume (given in voxels) for the particles before and after the thermal treatment and thus a volume evolution during the thermal treatment. The comparison of the areas obtained for both particles before and after the treatment reveals an important decrease of the well-defined faceted surfaces. By considering the total number of pixels identified as facets, we could calculate decreases of 17.5 % and 31 % of the total defined facets for the two analyzed particles and decreases of 9 % and 18 % from their initial volumes, respectively. These two particles, being present in the same silica shell, the faceting/size evolution was followed by a trend toward the sintering/coalescence phenomena (see the (xy) slices and the 3D volume, in insets). The (xy) slice of a single particle (last column, Figure 4) illustrates that a new quite round surface appears instead of the well-defined facets existing before the thermal treatment.

The Pd MTPs were found to display a better stability regarding the thermal treatment. Figure 5 illustrates the evolution of typical Pd MTPs from the area 2 via 2D images and (xy) slices extracted from the ET reconstructions of the same particles, before and after the thermal treatment. The 3D model obtained for a typical MTP (particle 1) confirms that the particle displays an icosahedral morphology, before and after the thermal treatment, with at least twelve facets (mixture of triangular and hexagonal shapes). To investigate the faceting and the morphology evolution, a similar quantitative analysis of the external faceting was performed on the particle 1, allowing comparing the type and the areas of the well identified facets (see Table 2SI and movies SI-5 and SI-6). This analysis

has shown that the morphology and faceting are generally well preserved during the thermal treatment, except to the fact that the facets areas are slightly smaller, in agreement with the small rounding of the particle. By considering the total number of pixels identified as facets, we could quantify 5% less of well-defined facets due to thermal treatment and a decrease of volume of about 3 %. No sintering phenomena were observed even when two particles (or more) are encapsulated in the same silica shell (see particles 2 in Figure 5).

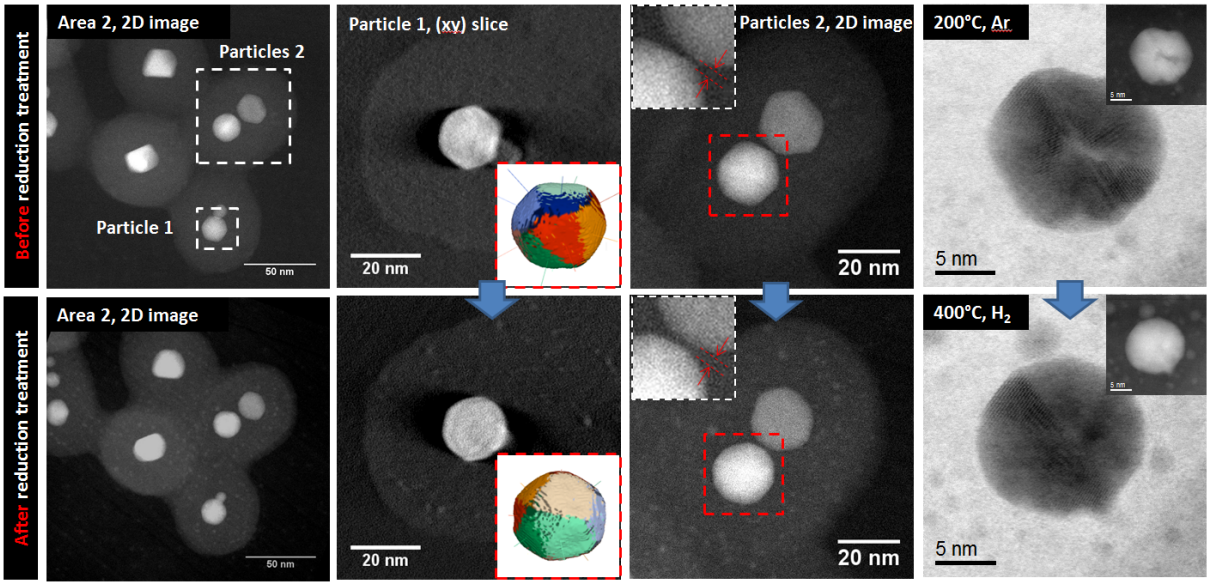

Figure 5. MTPs Pd before (*top*) and after (*bottom*) the thermal treatment: *From Left to right:* (1) STEM-ADF images of the area 2 with the two particles chosen for a more detailed analysis highlighted by white squares, (2) a typical slice through the reconstruction of the particle 1, with in insets the 3D models with the crystallographic facets, (3) STEM-ADF images of the particles 2, with in insets a more detailed view of the area between the two individual particles, (4) High resolution STEM-BF images of one typical MTP, inset the STEM-HAADF images.

In the literature, similar faceting dependence of the thermal stability was observed for Pd@Pt single-crystal particles treated at high temperature: cubic particles enclosed by (100) facets were found to be less stable and their shape readily deformed at a temperature 300 °C lower than the one of octahedral particles enclosed inside (111) facets.[42] In our case, the different behaviour of two Pd particles types can be explained by the fact that the MTPs display a majority of (111) facets with lower surface energy than the (100) facets present at the surface of the monocrystalline particles, which enhances the reactivity and the inter-diffusion of palladium through the Pd/SiO_2 interface in the case of the monocrystalline NPs. In order to investigate this hypothesis, a new sample of Pd@SiO_2, with a cubic core Pd NP, was thermally reduced *in situ* in the same conditions (Figure 5 SI). The presence of almost only (100) facets at the cubic Pd surface was found to significantly enhance the diffusion kinetics leading to the formation of a much larger number of new Pd particles within the silica shell and on its outer surface. In fact, previous studies via CO adsorbed DRIFT (Diffuse Reflectance Infrared Fourier Transform spectroscopy) realized at 400 °C on Pd@SiO_2 samples with Pd icosahedral and cubic shapes showed that the total proportion of (100) facets is higher in the Pd@SiO_2 containing cubic Pd than in the Pd@SiO_2 containing polyedric Pd (50% versus 39%).[30]

The better thermal stability of Pd MTPs can be also explained by the fact that such polycrystalline structures present more defects like grain boundaries, voids, vacancies, etc., and the thermal activated diffusion leads to “internal atom displacements” and less exchange with the external surface. Such a

hypothesis can be confirmed by analysing the high resolution STEM image in Figure 5 (last column), showing the MTP at 200 °C with a contrast revealing the presence of voids inside some regions, supposing that no chemical heterogeneities are present; at 400 °C the particle seems to be more homogeneous.

3. Behavior of Pd@SiO_2 nanostructures at high temperatures under H_2 and air

To provide additional information on the diffusion mechanism from the core during the reduction of Pd@SiO_2 nanostructures, two additional *in situ* E-TEM experiments were carried out: (1) a thermal treatment up to 400 °C under argon (Ar) followed by a thermal treatment under H_2 from 400 °C up to 1000 °C, (2) a thermal treatment up to 850 °C under air. These experiments were aimed at investigating the formation of the small particles within the silica shells up to 400 °C under different gas (Ar and air) and to study the thermal stability of the Pd@SiO_2 nanostructures under H_2 and air at high temperatures. Figure 6 illustrates the thermal evolution of typical Pd@SiO_2 particles during such treatments (more particles are present in Figure 6SI and 7SI).

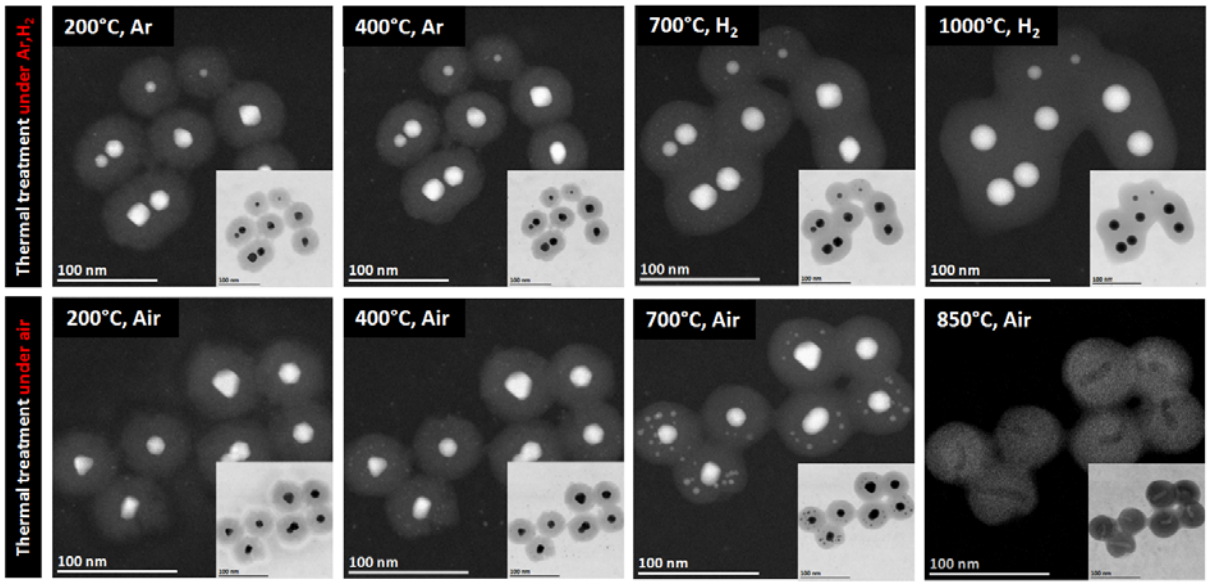

Figure 6. STEM-ADF images (in inset BF-STEM images) illustrating the evolution of typical Pd@SiO_2 particles during the *in situ* thermal treatment (*top*) up to 400 °C under Ar and then from 400 °C to 1000 °C under H_2 and (*bottom*) up to 850 °C under air.

For both *in situ* thermal treatment under argon and air, the images show a similar mechanism of small particles formation between 300 °C and 400 °C, which suggest that the coalescence and/or the diffusion of palladium process is thermally activated and does not depend upon the environment gas. Under H_2, starting from 400 °C the kinetics of palladium diffusion increases as a function of the temperature and additional small particles appeared up to 700 °C, whereas for higher temperatures we observed fewer particles inside the shell and only a few particles remain at 1000 °C. In fact, starting from 700°C the silica shells become denser due to partial reduction/shrinkage phenomena and such morphological transformations are expected to result in a decrease of the pores sizes until the formation of a non-porous dense layer (as observed at 1000 °C). As a result, the core Pd coalesces and completely loses its morphology, but remains "trapped" inside the shell; the small particles formed at 300 °C do diffuse conversely in the direction of the Pd core due to the closing of the porosity, some of them being encapsulated in the silica.

In the case of thermal treatment under air, the kept opened porosity allows to observe the enhancement of the diffusion kinetics of Pd from the core. At 500 °C, larger particles of about 3-4 nm

are formed on the external surface of silica and at 850 °C, the palladium completely disappeared and only void silica particles were observed due to a diffusion of the totality of the Pd cores through silica which still displays a porous microstructure (observed in STEM-ADF images at 850 °C). The *in situ* diffusion mechanism of palladium from the core was recorded between 700 °C and 850 °C (movie SI-7). The images extracted from this video (Figure 7SI) show a (1) continuous decreasing of the Pd core size, (2) the disappearance of small particles formed at 300 °C inside the shell accompanied by (3) the appearance/growth of new particles on the outer surface of silica. After the total diffusion of the Pd core and of the small particles inside the silica pores has taken place, the size of the new particles formed on the outer surface decreases down to their disappearance. The above *in situ* results do evidence that encapsulated Pd particles can completely redisperse/diffuse within the silica shell in the form of very small entities provided the presence of opened pores. Such total diffusion mechanism in $Pd@SiO_2$ was observed by C.Y. Seo et al. at 800 °C under a pressure of 150 Torr of O_2 with core Pd of about 5 nm.[37]

Conclusions

Herein, we report on the first quantitative application of a combined TEM-based approach of E-TEM at atmospheric pressure and Electron Tomography (ET), as a unique tool for investigating the 3D-dynamical evolution of materials or catalysts. Applied on the same objects, it provides correlative information on the particle morphology and crystallographic faceting on the one hand, and its evolution under thermal constraints in various gas environments on the other hand.

This approach was here applied for following the *in situ* reduction of $Pd@SiO_2$ particles using traditional experimental conditions (400 °C, H_2, 760 Torr). At 300 °C the formation of new Pd particles inside the silica shell is related to a diffusion-ripening mechanism of the clusters initially present inside the silica poresor of the atoms originating from the core Pd. The same behaviour was observed under Ar and air, thus demonstrating that the as-observed diffusion at medium temperature is thermally activated. In addition, thanks to the 3D approach by combining E-TEM and ET, we were able to precisely quantify the volume and the faceting evolution of the two kinds of studied Pd particles against their thermal treatment. We have shown higher thermal stability for icosahedral MTPs owing to lower diffusion at the Pd/silica surface, the atomic diffusion happening generally via the internal defects of such polycristalline structures. The octahedral particles were found to be less stable during the thermal treatment and exhibited a more efficient diffusion leading to a size decrease and a variation of the faceting. At higher temperatures, the stability of $Pd@SiO_2$ depends on the oxidative/reductive nature of gas environment. Under H_2, the silica lost its porosity and formed a dense layer at 700 °C, with the Pd at the core no more faceted but encapsulated in the shell up to 1000 °C. Under air, the porous structure of the silica is still stable, the diffusion mechanism of Pd from the core inside the silica pores increases as a function of temperature to form new particles on the external surface of silica up to 850 °C, temperature at which the whole the core was diffused.

Acknowledgements

Authors would like to thank the French ANR (National Research Agency) under the 3DCLEAN project 15-CE09-0009-01 for financial support.

Experimental methods

$Pd@SiO_2$ preparation

The $Pd@SiO_2$ nanostructures were synthesized following the procedure detailed in ref. **30** and consists in three steps: (1) a seed mediated growth of Pd particles from isotropic colloids of 3-4 nm following the Nikoobakht method,[43] (2) the Pd encapsulation by a mesoporous silica shell and (3) the thermal treatment at 250 °C under H_2.

Palladium NPs synthesis via a seed mediated growth method: 180 ml of a K_2PdCl_4 (2.7mM) solution was added to 150 ml of a hexadecyltrimethylammonium bromide (CTAB) 95 mM under stirring at 30 °C under H_2 atmosphere. Then, 6 ml of a sodium ascorbate 80 mM were added and the final solution was stirred at 30 °C for 4 h under H_2.

Silica shell growth: 300 ml of H_2O, 260 ml of EtOH and 3.5 ml of NH_4OH 28wt.% aqueous solution were added to the previous colloidal solution of nanoparticles.

In order to obtain core@shell Pd nanoparticles with a mesoporous silica shell ($Pd@m\text{-}SiO_2$), 1 g of tetraethylorthosilicate (TEOS) is added afterwards drop-wise under strong magnetic stirring and the mixture is left overnight for maturation under moderate stirring at room temperature.

After maturation and EtOH addition, the suspension was centrifuged (20 min, 14,000 rpm) to recover the precipitate.

Thermal treatment: The black solid is then dried under air at room temperature and finally treated with a hydrogen flow at 250 °C for 12 h (heating rate of 2 °C min^{-1}).

Transmission Electron Microscopy (TEM) and Scanning TEM (STEM)

Transmission electron microscopy (TEM) analysis was carried out using a JEOL 2100 FEG S/TEM microscope operated at 200 kV equipped with a spherical aberration corrector on the probe forming lens. For imaging, the samples were dispersed in ethanol and deposited on a holey carbon coated TEM grid. For scanning transmission electron microscopy (STEM) high-angular annular dark field (HAADF) analysis, a spot size of 0.13 nm, a current density of 140 pA, a camera focal length of 8 cm, corresponding to inner and outer diameters of the annular detector of about 73 and 194 mrad, were used. Elemental analyses were carried out with an energy dispersive X-ray spectroscopy (EDX) probe using a silicon drift detector (SDD) with a sensor size of 60 mm^2.

Environmental TEM

The $Pd@SiO_2$ sample was deposited onto a Protochip support (E-Chip)[44], which is a thin ceramic heating membrane controlled with the "Atmosphere" software in order to automatically adjust the temperature under different pressures and gas species. The sample was deposited on the heating membrane via sputtering through a thin slit directly above the membrane. A second cell chip with a SiN membrane is located on top of the thermal E-chip in the TEM holder, producing a thin gas cavity sealed with small o-rings maintaining the high vacuum in the TEM column.

During the experiment, the sample was observed and imaged at a pressure of 1 atm (760 Torr) of argon to localize the zones that will be observed later, then the gaz (Ar, H_2 or air) was introduced and the sample was heated to the desired temperatures.

Electron Tomography

In order to realize the Electron tomography (ET), the E-chip containing the sample was introduced and fixed inside the specific sample holder destined to the ET experiments. The acquisition of tilt

series was acquired using the tomography plug-in of the Digital Micrograph software, which controls the specimen tilt step by step, the defocusing and the specimen drift. The HAADF and BF tilt series in the STEM were acquired by using the ADF and BF detectors and tilting the specimen in the angular range of ± 51.5° using an increment of 1.5° in the equal mode, giving thus a total number of images equal to 69 images in each series. The inner radius of the ADF detector was about 40 mrad, a relatively large value that allows us to consider that the intensity in the corresponding images is proportional to the mean atomic number of the specimen in a first approximation.

The recorded images of the tilt series were spatially aligned by cross correlating consecutive images using IMOD software.[45] For the volume calculation, we have used the algebraic reconstruction technique (ART)[46] implemented in the TomoJ plugin[47] working in the ImageJ software[48] were thus used to compute the reconstructed volumes. Finally, the visualization and the analysis of the final volumes were carried out using the displaying capabilities and the isosurface rendering method in the Slicer software.[49]

Quantitative 3D analysis of the particle faceting

Quantitative analysis of the particles faceting is carried out as follows, using the DESK framework[50]: First, each particle surface is extracted and meshed using the ACVD software.[51] The result is a uniform mesh with 10000 vertices. A normal axes is estimated on each vertex. Then the normal axes are clustered into 20 classes using the K-means algorithm. In order to remove small non-planar regions, only the 14 biggest classes are kept. Finally, for each planar region, the vertices with a normal deviating less than 20 degrees from the region average are kept. This gives a robust vertex count for each planar region, and as the mesh is uniform, the number of vertices inside each planar region is a good approximation of the region area.

References

(1) Oh, S. H.; Hoflund, G. B. Chemical State Study of Palladium Powder and Ceria-Supported Palladium during Low-Temperature CO Oxidation. *J. Phys. Chem. A* **2006**, 110, 7609-7613.

(2) Venezia, A. M.; Liotta, L. F., Pantaleo, G.; Parola, V. L.; Deganello, G.; Beck, A.; Koppany, Z.; Frey, K.; Horvath, D.; Guczi, L. Activity of SiO_2 supported gold-palladium catalysts in CO oxidation. *Appl. Catal. A* **2003**, 251, 359-368.

(3) Gabasch, H.; Knop-Gericke, A.; Schlogl, R.; Borasio, M.; Weilach, C.; Rupprechter, G.; Penner, S.; Jenewein, B.; Hayek, K.; Klotzer, B. Comparison of the reactivity of different Pd–O species in CO oxidation. *Phys. Chem. Chem. Phys.* **2007**, 9, 533-540.

(4) Quincoces, C. E. ; Guerrero, S. ; Araya, P. ; Gonzalez, M. G. Effect of water vapor over Pd–Co/SZ catalyst for the NO selective reduction by methane. *Catal. Commun.* **2005**, 6, 75-80.

(5) Radev, L.; Khristova, M.; Mehandjiev, D.; Samuneva, B. Sol-gel Ag + Pd/SiO_2 as a catalyst for reduction of NO with CO. Catal. Lett. 2006, 112, 181-186.

(6) Jen, P. H.; Hsu, Y. H.; Lin, S. D. The activity and stability of Pd/C catalysts in benzene hydrogenation. *Catal. Today* **2007**, 123, 133–141.

(7) Panpranot, J.; Kontapakdee, K.; Praserthdam, P.; Selective hydrogenation of acetylene in excess ethylene on micron-sized and nanocrystalline TiO_2 supported Pd catalysts. *Appl. Catal. A* **2006**, 314, 128-133.

(8) Seth, D.; Sarkar, A.; Ng, F. T. T.; Rempel, G. L. Selective hydrogenation of 1,3-butadiene in mixture with isobutene on a Pd/α-alumina catalyst in a semi-batch reactor. *Chem. Eng. Sci.* **2007**,62, 4544–4557.

(9) Borade, R. B.; Zhang, B.; Clearfield, A. Selective dehydrogenation of cyclohexene to benzene using Pd-exchanged α-zirconium phosphate. *Catal. Lett.* **1997** 45, 233-235.

(10) Albers, P.; Pietsch, J.; Parker, S. F. Poisoning and deactivation of palladium catalysts. *J. Mol. Catal. A* **2001**, 173, 275-286.

(11) Grunwaldt, J. D.; Vegten, N. v.; Baiker, A. Insight into the structure of supported palladium catalysts during the total oxidation of methane. *Chem. Commun.* **2007**, 0, 4635-4637.

(12) Chou, J.; Zhang, S.; Sun, S.; McFarland, E. W. Benzene Formation at 70 °C by Coupling of Propylene on Supported Pd Nanoclusters. *Angew. Chem. Int. Ed.* **2005**, 44, 4735-4739.

(13) Budroni, G.; Corma, A.; Garcıa, H.; Primo, A. Pd nanoparticles embedded in sponge-like porous silica as a Suzuki–Miyaura catalyst: Similarities and differences with homogeneous catalysts. *J. Catal.* **2007**, 251, 345–353.

(14) Wilson, O. M.; Knecht, M. R.; Garcia-Martinez, J. C.; Crooks, R. M.; Effect of Pd Nanoparticle Size on the Catalytic Hydrogenation of Allyl Alcohol. *J. Am. Chem. Soc.* **2006**, 128, 4510-4511.

(15) Lu, A. H.; Li, W. C.; Hou, Z.; Schuth, F. Molecular level dispersed Pd clusters in the carbon walls of ordered mesoporous carbon as a highly selective alcohol oxidation catalyst. *Chem. Commun.*, **2007**,0, 1038-1040.

(16) Wang, Y.; Lee, J. K. Recyclable nano-size Pd catalyst generated in the multilayer polyelectrolyte films on the magnetic nanoparticle core. *J. Mol. Catal. A* **2007**, 263, 163–168.

(17) Liu, R. J.; Crozier, P. A.; Smith, C. M.; Hucul, D. A.; Blackson, J.; Salaita, G. Metal sintering mechanisms and regeneration of palladium/alumina hydrogenation catalysts. *Appl. Catal. A* **2005**, 282, 111-121.

(18) Cargnello, M.; Wieder, N. L.; Montini, T.; Gorte, R. J.; Fornasiero, P. Synthesis of Dispersible $Pd@CeO_2$ Core–Shell Nanostructures by Self-Assembly. *J. Am. Chem. Soc.* **2010**, 132, 1402-1409.

(19) Bakhmutsky, K.; Wieder, N. L.; Cargnello, M.; Galloway, B.; Fornasiero, P.; Gorte, R. J. A Versatile Route to Core–Shell Catalysts: Synthesis of Dispersible M@Oxide (M=Pd, Pt; Oxide=TiO_2, ZrO_2) Nanostructures by Self-Assembly. *ChemSusChem* **2012**, 5, 140-148.

(20) Zhang, N. ; Liu, S. Q. ; Fu, X. Z. ; Xu, Y. J. Synthesis of $M@TiO_2$ (M = Au, Pd, Pt) Core–Shell Nanocomposites with Tunable Photoreactivity. *J. Phys. Chem. C* **2011**, 115, 9136-9145.

(21) Bae, D. S.; Han, K. S.; Adair, J. H. Synthesis and microstructure of Pd/SiO_2 nanosized particles by reverse micelle and sol–gel processing. *J. Mater. Chem.* **2002**, 12, 3117-3120.
(22) Park, J. N.; Forman, A. J.; Tang, W.; Cheng, J.; Hu, Y. S.; Lin, H.; McFarland, E. W. Highly Active and Sinter-Resistant Pd-Nanoparticle Catalysts Encapsulated in Silica. *Small* **2008**, 4, 1694-1697.
(23) Cargnello, M.; Jaen, J. J. D.; Garrido, J. C. H.; Bakhmutsky, K.; Montini, T.; . Gamez, J. J. C.; Gorte, R. J.; Fornasiero, P. Exceptional activity for methane combustion over modular $Pd@CeO_2$ subunits on functionalized Al_2O_3. *Science* **2012**, 337, 713-717.
(24) Liu, R. J.; Crozier, P. A.; Smith, C. M.; Hucul, D. A.; Blackson, J.; Salaita, G. In Situ Electron Microscopy Studies of the Sintering of Palladium Nanoparticles on Alumina during Catalyst Regeneration Processes. *Microsc. Microanal.* **2004**, 10, 77.
(25) Batail, N.; Clémençon, I.; Legens, C.; Chaumonnot, A.; Uzio, D. Controlled Synthesis and High Oxidation Stability of Cobalt Nanoparticles Encapsulated in Mesoporous Silica using a Modified Stöber Approach and a Pseudomorphic Transformation. *Eur. J. Inorg. Chem.* **2013**, 8, 1258–1264
(26) Joo, S. H.; Park, J. Y.; Tsung, C. K.; Yamada, Y.; Yang, P.; Somorjai, G. A. Thermally stable Pt/mesoporous silica core-shell nanocatalysts for high-temperature reactions. *Nat. Mater.* **2009**, 8, 126.
(27) Li, K. T.; Hsu, M. H.; Wang, I. Palladium core–porous silica shell-nanoparticles for catalyzing the hydrogenation of 4-carboxybenzaldehyde. *Catal. Commun.* **2008**, 9, 2257-2260.
(28) Takenaka, S.; Orita, Y.; Umebayashi, H.; Matsune, H.; Kishida, M. High resistance to carbon deposition of silica-coated Ni catalysts in propane stream reforming. *Appl. Catal. A* **2008**, 351, 189-194.
(29) Shin, S.; Yoon, H.; Jang, J. Polymer-encapsulated iron oxide nanoparticles as highly efficient Fenton catalysts. *Catal. Commun.* **2008**, 10, 178-182.
(30) Martins, J.; Batail, N.; Silva, S.; Rafik-Clement, S.; Karelovic, A.; Debecker, D.P.; Chaumonnot, A.; Uzio, D. CO_2 hydrogenation with shape-controlled Pd nanoparticles embedded in mesoporous silica: Elucidating stability and selectivity issues. *Catal. Commun.* **2015**, 58, 11–15.
(31) Dembele, K.; Moldovan, S.; Hirlimann, C.; Harmel, J.; Soulantica, K.; Serp, P.; Chaudret, B.; Gay, A.S.; Maury, S.; Berliet, A.; Fecant, A.; Ersen, O. Reactivity and structural evolution of urchin-like Co nanostructures under controlled environments. *Journal of Mircoscopy* **2017**, 0, 1-9.
(32) Han, L.; Meng, Q.; Wang, D.; Zhu, Y.; Wang, J.; Du, X.; Stach, E. A.; Xin, H. L. Interrogation of bimetallic particle oxidation in three dimensions at the nanoscale. *Nature Communications* **2016**, 7, 13335.
(33) Roiban, L.; Koneti, S.; Tran, K.; Feng, Y. M.; Grenier, T.; Maxim, V.; Epicier, T. Rapid Tomography in Environmental TEM: How Fast Can We Go to follow the 3D Evolution of Nanomaterials in situ? *Microsc. Microanal.* **2016**, 22 (Suppl 5).
(34) Xiong, Y.; McLellan, J. M.; Yin, Y.; Xia, Y. Synthesis of Palladium Icosahedra with Twinned Structure by Blocking Oxidative Etching with Citric Acid or Citrate Ions. Angew. Chem., Int.Ed. 2007, 46, 790-794.
(35) Berhault, G.; Bausach, M.; Bisson, L.; Becerra, L.; Thomazeau, C.; Uzio, D.; Seed-Mediated Synthesis of Pd Nanocrystals: Factors Influencing a Kinetic- or Thermodynamic-Controlled Growth Regime. *J. Phys. Chem. C* **2007**, 111, 5915-5925.
(36) Forman, A. J.; Park, J. N.; Tang, W.; Hu, Y. H.; Stucky, G. D.; McFarland, E. W. Silica-Encapsulated Pd Nanoparticles as a Regenerable and Sintering-Resistant Catalyst. *ChemSusChem* **2010**, 2, 1318-1324.
(37) Seo, C. Y.; Chen, X.; Sun, K.; Allard, L. F.; Fisher, G. B.; Schwank, J. W. Palladium redispersion at high temperature within the $Pd@SiO_2$ core@shell structure. *Catal. Commun.* **2018**, 108, 73-76.
(38) Sietsma, J. R. A.; Meeldijk, J. D.; den Breejen, J. P.; Versluijs-Helder, M.; van Dillen The Preparation of Supported NiO and Co3O4 Nanoparticles by the Nitric Oxide Controlled Thermal Decomposition of Nitrates. *Angew. Chem. Int. Ed.* **2007**, 46, 4547-4549.
(39) Min, B. K.; Santra, A. K.; Goodman, D.W. Understanding silica-supported metal catalysts: Pd/silica as a case study. *Catal. Today* **2003**, 85, 113–124.

(40) Tew, M. W.; Miller, J. T.; van Bokhoven J. A. Particle Size Effect of Hydride Formation and Surface Hydrogen Adsorption of Nanosized Palladium Catalysts: L3 Edge vs K Edge X-ray Absorption Spectroscopy. *J. Phys. Chem. C,* **2009**, 113, 15140–15147.
(41) Narayan, T. C.; Hayee, F.; Baldi, A.; Koh, A. L. Sinclair, R.; Dionne, J. A. *Nature Communications*, 8, **2017**, 14020.
(42) Vara, M.; Roling, L. T.; Wang, X.; Elnabawy, A. O.; Hood, Z. D.; Chi, M.; Mavrikakis, M.; Xia, Y. Understanding the Thermal Stability of Palladium–Platinum Core–Shell Nanocrystals by In Situ Transmission Electron Microscopy and Density Functional Theory. *ACS Nano*, **2017**, 11, 4571-4581.
(43) Nikoobakht, B.; El-Sayed, M. A. Preparation and Growth Mechanism of Gold Nanorods (NRs) Using Seed-Mediated Growth Method. *Chem. Mater.* **2003**, 15, 1957-1962.
(44) www.Protochips.com
(45) Mastronarde, D. N. Dual-axis tomography: an approach with alignment methods that preserve resolution. *J. Struct. Biol.* **1997**,120, 343−352.
(46) Gordon, R.; Bender, R.; Herman, G. T. Algebraic reconstruction techniques (ART) for three-dimensional electron microscopy and x-ray photography. *J. Theor. Biol.* **1970**, 29,471− 481
(47) Messaoudii, C.; Boudier, T.; Schancez Sorzano, C. O.; Marco, S. BMC Bioinf. 2007,6, 288−292
(48) http://u759.curie.u-psud.fr/softwaresu759.html.
(49) http://www.Slicer3D.org.
(50) Jacinto, H.; Kéchichian, R.; Desvignes, M.; Prost, R.; Valette, S. A Web Interface for 3D Visualization and Interactive Segmentation of Medical Images, in 17th International Conference on 3D Web Technology (Web 3D 2012), Los-Angeles, USA, 2012, p. 51-58.
(51) Valette, S.; J. M.; Chassery, Prost, R. Generic remeshing of 3D triangular meshes with metric-dependent discrete Voronoi Diagrams. *IEEE Trans Visu Comp Grap*, **2008**, 14, 369–381.